High entropy lithium garnets – Testing the compositional flexibility of the lithium garnet system

Stockham, Mark; Dong, Bo; Slater, Peter

DOI:
10.1016/j.jssc.2022.122944

Document Version
Publisher's PDF, also known as Version of record

Citation for published version (Harvard):
Stockham, M, Dong, B & Slater, P 2022, 'High entropy lithium garnets – Testing the compositional flexibility of the lithium garnet system', *Journal of Solid State Chemistry*, vol. 308, 122944.
https://doi.org/10.1016/j.jssc.2022.122944

Journal of Solid State Chemistry 308 (2022) 122944

Contents lists available at ScienceDirect

Journal of Solid State Chemistry

journal homepage: www.elsevier.com/locate/jssc

High entropy lithium garnets – Testing the compositional flexibility of the lithium garnet system

Mark P. Stockham *, Bo Dong, Peter R. Slater **

School of Chemistry, University of Birmingham, Birmingham, B15 2TT, UK

ARTICLE INFO

Keywords:
Lithium garnet
High entropy
Solid state batteries
Solid state electrolytes

ABSTRACT

There is a pressing need for higher energy density, safer batteries for electric vehicles and grid energy storage. The current consensus is that these batteries need to be replaced with fully solid equivalents, however the discovery of a suitable solid state electrolyte has proven troublesome. Of the promising materials, lithium garnets are popular due to their wide electrochemical window, good ionic mobility (>0.1 mS cm^{-1}) and compatibility with Li metal. However, numerous issues remain relating to interfacial resistance, time consuming and energy demanding synthesis and special handling requirements to ensure the best performing membranes. Of these challenges, little work has been done on the effect of entropy in the cubic lithium garnet systems, for example by addition of multiple elements on multiple sites. Such strategies have given interesting results in other areas (e.g. battery cathodes, metal alloys) and could well enable better performing membranes by increasing the, already high, disorder and take advantage of the numerous dopants reports which often singularly enable favourable properties (such as increased density, higher conductivity, lower interfacial resistance). Herein we test the compositional flexibility of the lithium garnet system with a 9 ($Ga_{0.2}Li_{5.75}La_{2.5}Nd_{0.5}Nb_{0.65}Ce_{0.1}Zr_1Ti_{0.25}O_{12}$) and 11 ($Ga_{0.2}Li_{5.75}La_{2.5}Nd_{0.5}Nb_{0.35}Ta_{0.3}Ce_{0.1}Zr_{0.75}Hf_{0.25}Ti_{0.25}O_{12}$) element system. Surprisingly, we did not find the limit of the garnet system, rather it was shown that (outside of the stoichiometric weighing) these systems were easy to synthesise, had high room temperature conductivity (0.2 mS cm^{-1}), and high density even when processed in air.

1. Introduction

Lithium solid state batteries are considered the holy grail of energy storage, encompassing higher energy densities and increased safety compared with conventional battery systems [1–7]. This, therefore, is thought to enable the ability to meet the power demands of modern society, especially in relation to electric vehicles and effective grid energy storage. Lithium-ion batteries (LIBs) are the energy storage system of choice, however currently they have significant drawbacks relating to electrolyte toxicity and flammability (commonly $LiPF_6$ in carbonate-based solvents). These electrolytes also give narrow electrochemical windows and lead to dendrite growth issues with Li metal anodes [1,2,8–10]. The electrolyte, however, remains the only component left to be replaced with a solid counterpart, and its replacement is the primary challenge in realising the next-generation energy storage [5,11–13].

The replacement of the electrolyte with a solid equivalent has proved exceptionally challenging, and of the available inorganic materials analysed (ranging from sulphides and oxides) most have either poor ionic conductivity or a narrow electrochemical window. Further challenges are also observed amongst these systems, with harder (oxide) materials exhibiting poor solid-solid contact at the electrode/electrolyte interface, while softer (sulphide) materials have better contact but have lower upper voltage stability along with extreme moisture sensitivity. Solid state electrolytes (SSE) also have complex, often non-scalable, synthesis strategies and are commonly analysed in a pellet type form which is of little commercial use. Hence, much work is still required.

Of the available SSEs, lithium garnets have seen high interest within the research community. Lithium garnets offer high conductivity (>0.1 mS cm^{-1}), a wide electrochemical window and chemical compatibility with Li metal. However, garnets are time consuming to synthesise and purify, need special requirements to obtain the highest performing membranes, suffer from high interfacial resistance (a large portion of which relates to Li^+/H^+ exchange) and have had issues transitioning to the thin film regime [14–20]. Of late, there has no reports, to our knowledge, of new high entropy garnets (HEG), which are designed to

* Corresponding author. School of Chemistry, University of Birmingham, Birmingham, B15 2TT, UK.
** Corresponding author. School of Chemistry, University of Birmingham, Birmingham, B15 2TT, UK.
E-mail address: mps846@student.bham.ac.uk (M.P. Stockham).

https://doi.org/10.1016/j.jssc.2022.122944
Received 9 December 2021; Received in revised form 20 January 2022; Accepted 25 January 2022
Available online 29 January 2022

maximise disorder and increase performance, thus opening new engineering approaches to garnet battery challenges.

A typical lithium garnet is cubic with space group Ia $\overline{3}$ d, such as $Li_5La_3Nb_2O_{12}$, with the exception of $Li_{7-x}Ga_xLa_3Zr_2O_{12}$ (Ga-LLZO) which is thought to adopt I4 $\overline{3}$ d type symmetry [21–24]. Li content needs to be > 5 per formula unit (*pfu*) to form a highly conductive garnet system but must remain <7 Li *pfu* to maintain the cubic structure. Those systems with 7 li *pfu*, such as $Li_7La_3Zr_2O_{12}$ (LLZO), form the thermodynamically stable $I4_1/acd$ system which is poorly conductive due to Li ordering reducing charge carrier mobility [21,25,26]. Therefore, most garnet reports concentrate on Li contents between 6 and 6.6 *pfu*, with aims to increase Li content in Li_5 based systems or Li removal with Li_7 systems. This is usually seen in the form of $Li_{5+x}La_3B_{2-x}M_xO_{12}$ (B = Nb, Ta, Zr, Hf, M = Pr, Ce, Ti, Ta, Nb) or $Li_{7-x}M_xLa_3B_2O_{12}$ (M = Al, Ga, Ge, B = Zr, Hf) [14,19,27–34]. Such strategies maintain the disordered Li sublattice and hence high conductivity [21].

Cubic lithium garnet systems, especially those with high Li content, may be considered highly entropic systems due to the Li disorder. It is, therefore, logical to conclude that increased entropy, via multiple dopant addition to several sites, may improve performance. In other areas, there are reports of high entropy alloys (≥ 5 elements), where such strategies can lead to materials with exceptional mechanical, magnetic, and electrical properties [35–44]. Such increasingly complex solid solutions were initially suggested to be stabilised by the entropic contribution to the total free energy and thus overcoming the enthalpic contribution [38], although it is now thought to be somewhat more complex [39]. The high entropy approach has also recently been explored with high entropy cathode materials (batteries and solid oxide fuel cells) which show increased capacity, improved ionic transport and superior rate capability [45–48]. This, therefore, shows the applicability of this approach to the energy storage field which could be, perhaps, quite a harmonious strategy if used with something as disordered as the cubic lithium garnets – whereby the deliberate entropic increases could be considered energetically favourable.

Herein we apply these concepts to lithium garnet materials with the idea that deliberate entropic increases could enable better performing garnet materials. This work aims to test the compositional flexibility of the garnet systems to enable strategic exploitation of numerous favourable dopant properties (e.g. increased density, improved conductivity) simultaneously. We designed two garnet systems based upon the commonly reported dopants elsewhere, with Zr (primary component of most garnet research), Nb and Ta (from the first garnet electrolyte report) [49], and Ti (Li dendrite suppression) [50]. We also encompass our prior work with Ce (increased conductivity, lower interfacial resistance), Ga/Nd (low interfacial resistance, high density) and Hf (possible increased electrochemical stability compared to Zr) [32,51–55]. Ga was also added to promote a symmetry alteration to the acentric I4 $\overline{3}$ d space group, as the exceptional performance of Ga-LLZO has been suggested to arise from the unique symmetry [24]. This, however, reduced Li content to 5.75 *pfu* (efforts to form a $Ga_{0.15}$ system and so prepare a $Li_{6.05}$ system were unsuccessful, see SI). The synthesised formulas were $Ga_{0.2}Li_{5.75}La_{2.5}Nd_{0.5}Nb_{0.65}Ce_{0.1}Zr_1Ti_{0.25}O_{12}$ (HEG1) and $Ga_{0.2}Li_{5.75}La_{2.5}Nd_{0.5}Nb_{0.35}Ta_{0.3}Ce_{0.1}Zr_{0.75}Hf_{0.25}Ti_{0.25}O_{12}$ (HEG2).

These materials, despite their considerable complexity, were easy to synthesise (outside of weighing of the chemicals) and showed good conductivity of ~0.2 mS cm^{-1} at room temperature, an impressive figure for a garnet system with less than 6 Li per formula unit and shows the dopant incorporation is favourable. This shows the tolerance of the garnet system to considerable doping strategies beyond the common single or co-doped route, the latter of which has already been suggested optimal for Li garnet performance due to multiple site disorder [56]. Given the success, there are multiple possible modifications that can be made in the future. It is hoped such strategies will open up new possibilities and enable fresh approaches to the engineering challenges of solid state batteries.

2. Methods

2.1. Synthesis

HEG1 and HEG2 were prepared via the solid-state route from stochiometric quantities of Li_2CO_3, Nd_2O_3, La_2O_3, Nb_2O_5, Ta_2O_5, ZrO_2, HfO_2, TiO_2, CeO_2 and Ga_2O_3 in air. A 40% mol excess of lithium was added to compensate for lithium loss during high temperature sintering. All powders were ball milled for 1 h with ZrO_2 balls (500 rpm) with hexane. The powder was then removed, dried and heated to 950 °C (12 h) at 5 °C min^{-1}.

2.2. Characterisation

Scanning electron microscopy (SEM) was performed on a Hitachi TM4000plus instrument. Elemental analysis was undertaken via an AZtecOne X-stream2 energy dispersive X-ray (EDX) spectrometer. Samples were prepared by applying the powders to a carbon tape and analysed at 15 kV in backscattered electron mode. Phase analysis was performed by X-ray diffraction (XRD) using a Bruker D8 diffractometer with a Cu X-ray source, with a step size of 0.02° and a total scan time of 12h. Experimental pellet densities were determined gravimetrically and compared to theoretical values from Rietveld refinement results (performed using the GSAS II software) [57].

2.3. Impedance spectroscopy

HEG1 and HEG2 were pelletised and densified in a dry room with a dewpoint between −45 °C and −64 °C (the elimination of humidity is known to be beneficial for high quality samples as moisture is an issue with Li garnet systems) [58–60]. Pellets were prepared as follows: approx. 10 mm diameter pellets were pressed to ca. 1.5 tonnes and heated to 1150 °C for 13 h (2 °C min^{-1}). Sacrificial powders were used to protect pellets from Al contamination from the Al_2O_3 crucible. Post-sintering, the pellets were polished and sputtered with Au for room temperature impedance spectroscopy measurements, which were performed with a Solartron 1260 impedance analyser from 1 Hz to 10 MHz with a 20 mV potential. All variable temperature measurements were undertaken from 25 to 117 °C. Variable temperature measurements required painting the pellet with Au electrodes and attaching of Au wires. The pellet was then heated (in air) to 800 °C (1h) to cure the Au paste. The pellets were then air quenched to room temperature from >700 °C (to limit H^+/Li^+ exchange [61–63]).

2.4. Cell assembly

All cell tests were performed on a biologic SP50 instrument. Li|HEG|Li symmetric cells were assembled in an Ar glove box. Pellets (~1 mm thickness) were polished using silicon carbide sandpaper from 240 to 4000 grit, then lithium metal foil was applied to each side of the pellet. The cell was then heated to 175 °C under a constant pressure for 1 h using a steel 3-way G clamp (see SI) and were secured under light pressure via hand tightening the clamp. The cell was subsequently secured in a MTI split test cell. Cells were examined via impedance spectroscopy before cell testing from 10 MHz to 0.1 Hz with a 20 mV potential on a Solartron 1260 impedance analyser. These symmetric cells were then cycled under constant current conditions at various current densities to assess cycling stability at 30 °C in a Genlab classic oven. Each cell cycle was 30 min (15 min each for Li stripping and plating), with a 10 s rest in between. At the lowest current density (12.5 μA cm^{-2}) the cell was cycled 200 times. At all other current densities cells were cycled 300 times. The temperature was monitored additionally via a Fluke 51 II external thermocouple.

3. Results and discussion

3.1. X-ray diffraction

The PXRD patterns of HEG1 and HEG2 are available in Fig. 1 and both were assumed to adopt the Ia $\overline{3}$ d type symmetry, although some small peaks were present in the latter ~22 θ. This peak was not well resolved and absent within HEG1, hence is ascribed to minor amounts of unreacted Li_2CO_3. Therefore, both phases were assumed to be Ia $\overline{3}$ d. Both systems demonstrate near phase pure symmetry, with some very minor background peaks present especially in HEG2, see Fig. 1. These relate to small Li–Ti–O and Li–Nb–O based impurities, however, when the material was heated to densify the pellet, these were readily removed and gave phase pure garnet material. This, therefore, indicates slightly longer sintering times are required for the powder. See Fig. 2.

Rietveld refinements were based upon the structural model from Hamao et al. (Ta-LLZO) [64]. The I4 $\overline{3}$ d model from Wagner et al. was also considered for the HEG2 pattern but the R factors were similar, so in the final refinement the former model was used for both [24]. The similarities in scattering factor on both the Ln site (La, Nd) and, for the most part, the B site (Ti, Zr, Nb, Ta, Hf, Ce) preclude the possibility of refining fractional occupancies. Although Ti and Ce are noticeable exclusions and could be refined, the inability to assess which corresponding B site element changes makes this impractical. Therefore, all elements were set to their intended ratios and not refined further. An example refinement is available in Fig. 3.

Lattice parameters for both systems were smaller than reports of other cubic garnet systems, such as. Ga/Al-LLZO (~13 Å) or Ta-LLZO (~12.94 Å) This corresponds to Ln contraction arising from Nd substitution, see Table 1. HEG2 has an especially high relative density (94%) which is suspected to arise from the Ln contraction and the Ga dopant, as we have shown prior [51]. This, therefore, confirms dopant property exploitation. HEG1, however, is somewhat lower (88%). This could indicate that density has increased with increased entropy, but perhaps is more likely related to the Ta and/or Hf dopants in HEG2. A more accurate understanding of such complex systems will not be a trivial task and will require synchrotron-based techniques and/or neutron diffraction, to more fully understand how substitution to this level affects the local structure.

XRD of HEG2 in pelletised form confirmed annealing removed the small impurities, as marked in Fig. 1. The XRD pattern showed formation of a phase pure product, with Rietveld refinements showing a small increase in lattice parameters to 12.8772(1) Å. Hence the minor background peaks are thought to relate to insufficient sintering time and unreacted Li_2CO_3. This was confirmed when HEG2 was re-synthesised and shown to require 14 h at 950 °C for phase purity, see SI. This is somewhat surprising as even singularly doped garnets (such as Al-LLZO, Ga-LLZO and Ta-LLZO) often suffer from synthesis strategies that require multiple grinding and heat treatment steps. Whereas HEG1 and HEG2 were pure immediately and on the very first synthesis (and remained easy to form upon repeat). It is, therefore, shown that compositional complexity of the garnet system aids in synthesis, however, comes at the cost of arduous weighing of the chemicals. Furthermore, with HEG1, attempts were made to reduce Ga content to 0.15 *pfu* and so prepare $Ga_{0.2}Li_{5.75}La_{2.5}Nd_{0.5}Nb_{0.65}Ce_{0.1}Zr_1Ti_{0.25}O_{12}$ (HEG1A). This was unsuccessful, showing multiple unknown impurities which were unable to be removed by further regrinding and heating, see SI.

3.2. SEM/EDX

The phase pure powder and pellet were subsequently analysed via SEM and EDX to assess elemental composition. Considering the similarities between the two systems only the more complex of the two was analysed, HEG2. The samples were analysed on a carbon tape in secondary electron mode (pellet), see Fig. 4. The EDX shows a mostly homogenous elemental distribution, with all elements detected (excluding Li) across the analysed sample. The EDX data suggests some areas of increased Ga concentration, which is in line with our own work on $Ga_{0.2}Li_{6.4}Nd_3Zr_2O_{12}$ [20,51], indicating further dopant exploitation will be achieved when assessed in symmetry cell format (see later) [52,65]. Outside of this, no Al contamination from the Al_2O_3 crucible was detected, despite no protection during sintering. Back scattered electron

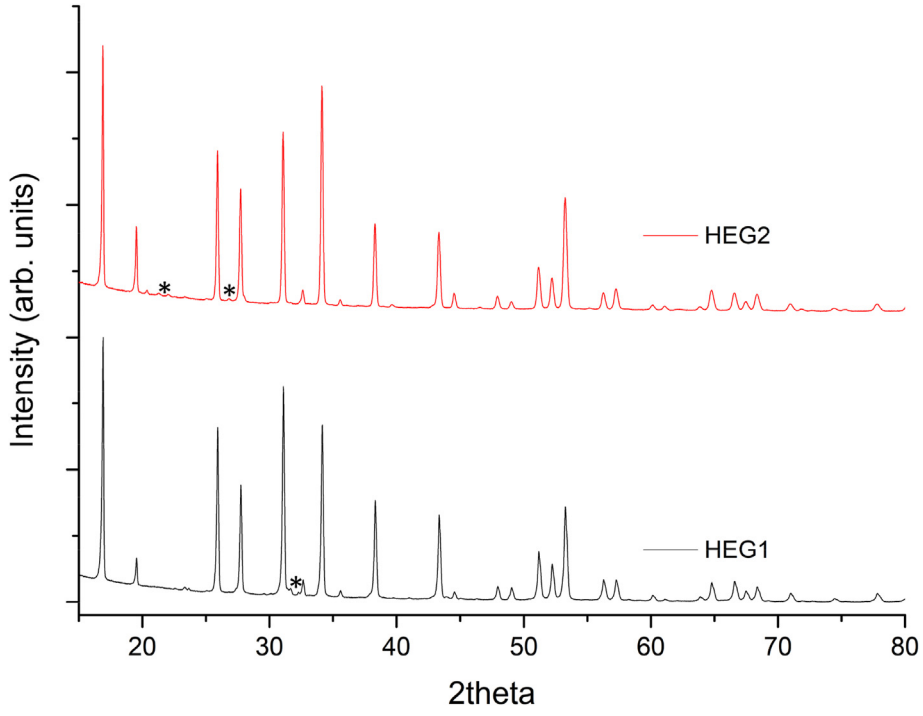

Fig. 1. PXRD patterns of HEG1 and HEG2, minor background impurities marked with stars and relate to Li based impurities which were removed upon annealing or sintering for 14h (rather than 12h). See SI. Both phases were indexed on Ia $\overline{3}$ d type symmetry.

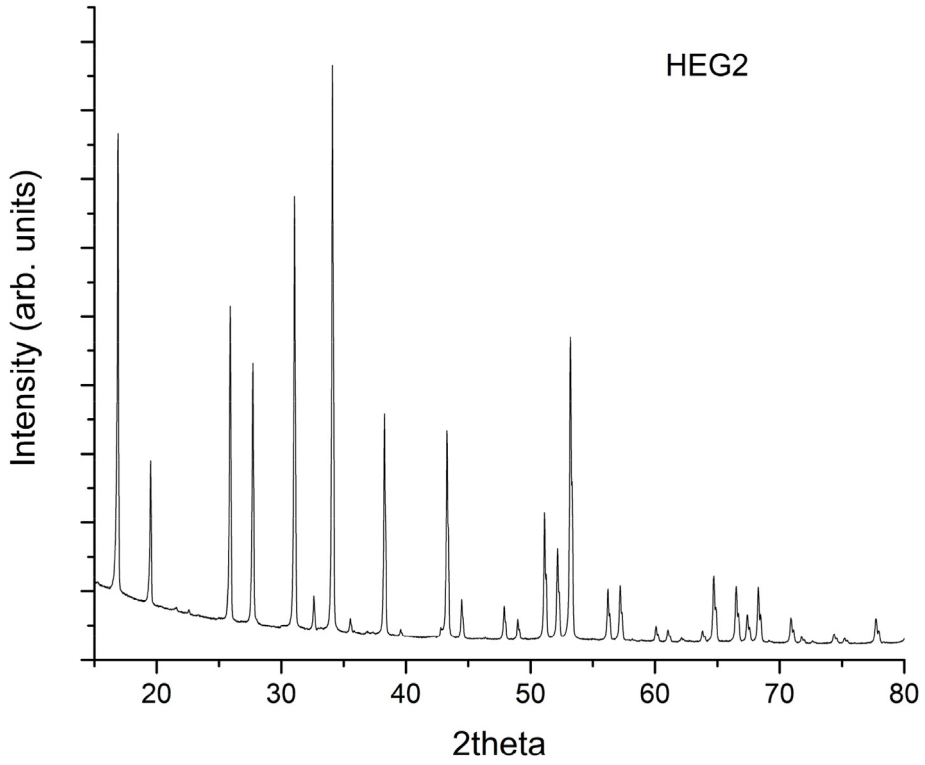

Fig. 2. PXRD pattern HEG2 post pellet densification at 1150 °C, showing removal of minor impurities the phase was indexed on Ia $\bar{3}$ d type symmetry and had a small lattice parameter increase when compared Fig. 1. Although an additional peak remains which could indicate I4 $\bar{3}$ d type symmetry refinements based on either crystal system yield highly similar lattice parameters, hence only Ia$\bar{3}$ d results were tabulated.

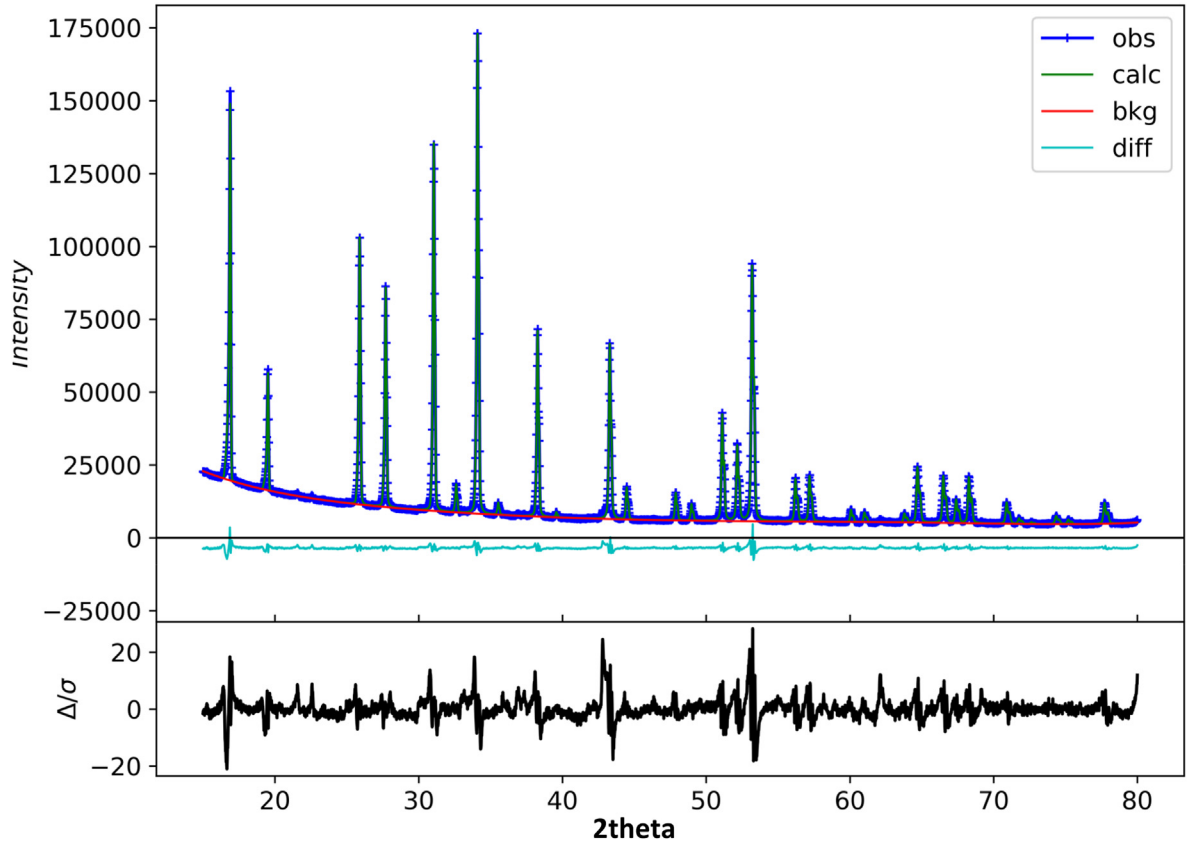

Fig. 3. Example Rietveld refinement of HEG2 based on the structural model of Ta-LLZO from Hamao et al. [64].

Table 1
Rietveld refinement and impedance spectroscopy data. Conductivity values for HEG1 take into consideration the additional grain boundary buried contribution. Further information on the calculation of capacitance and fitted values can be found in the SI.

Sample	Lattice parameters (Å)	σ_{total} (mS cm^{-1})	C_{bulk} (F/cm)	ε_r	C_{gb}(F/cm)	ρ_{rel} (%)
HEG1	12.8624(2)	0.1	5.2×10^{-12}	59	8.5×10^{-8}	88
HEG2	12.8720(3)	0.2	4.7×10^{-12}	53	–	94

images and EDX images of the powder are available in the SI, these show more prominent Ga dopant exsolution.

3.3. Impedance spectroscopy

HEG1 and HEG2 were Au Sputtered and analysed via impedance spectroscopy at room temperature (25 °C) to assess conductivity. Nyquist impedance plots for both samples are shown in Fig. 5a and b. For the less dense HEG1 (Fig. 5a) a clear bulk response is present, however there is a partially buried second response, likely relating to the grain boundary resistance. This is evidenced by the equivalent circuit, which required

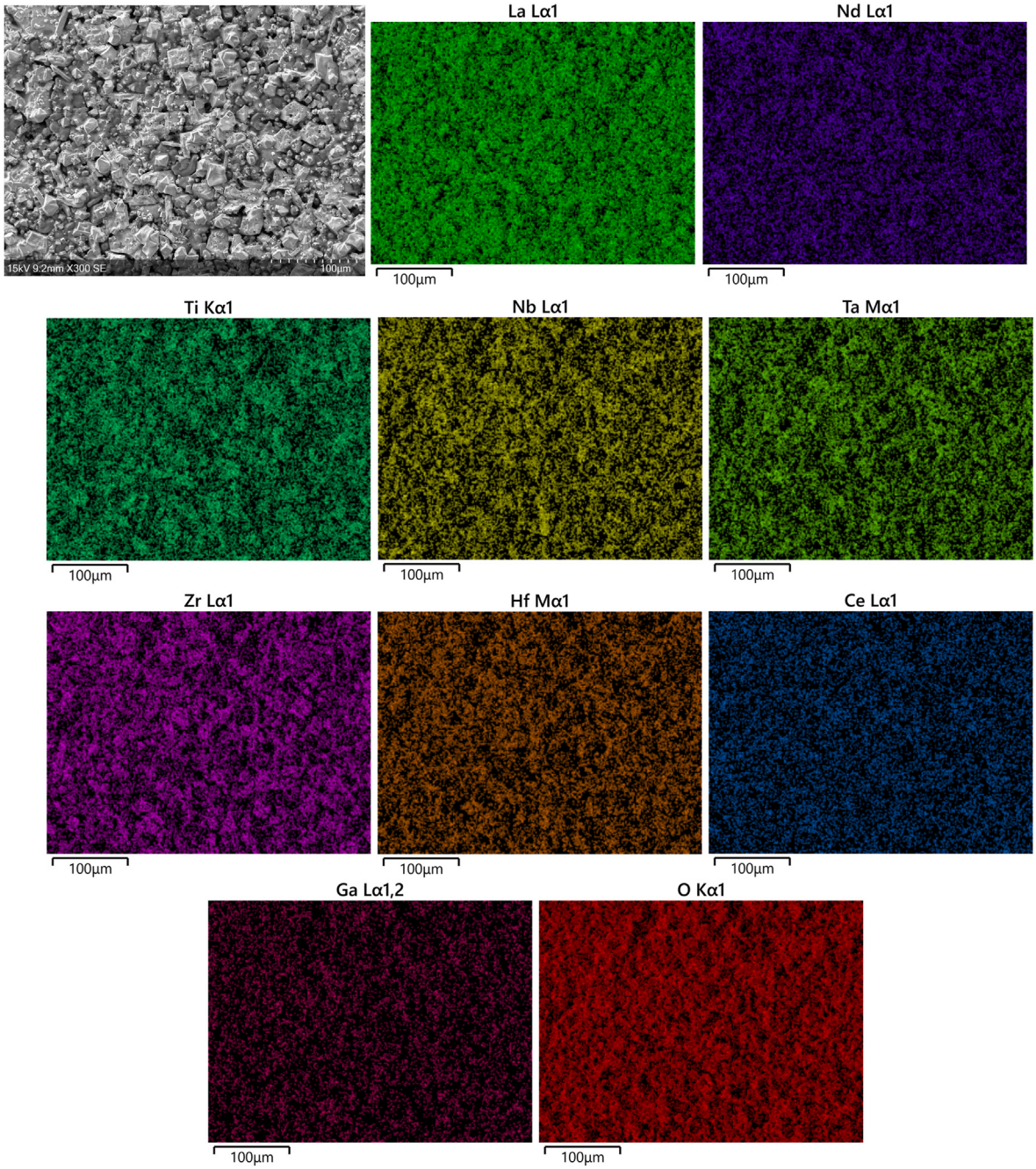

Fig. 4. SEM and EDX of HEG2 pellet surface, showing a relatively homogenous elemental distribution of HEG2 with some areas of higher elemental concentrations, particularly Ga.

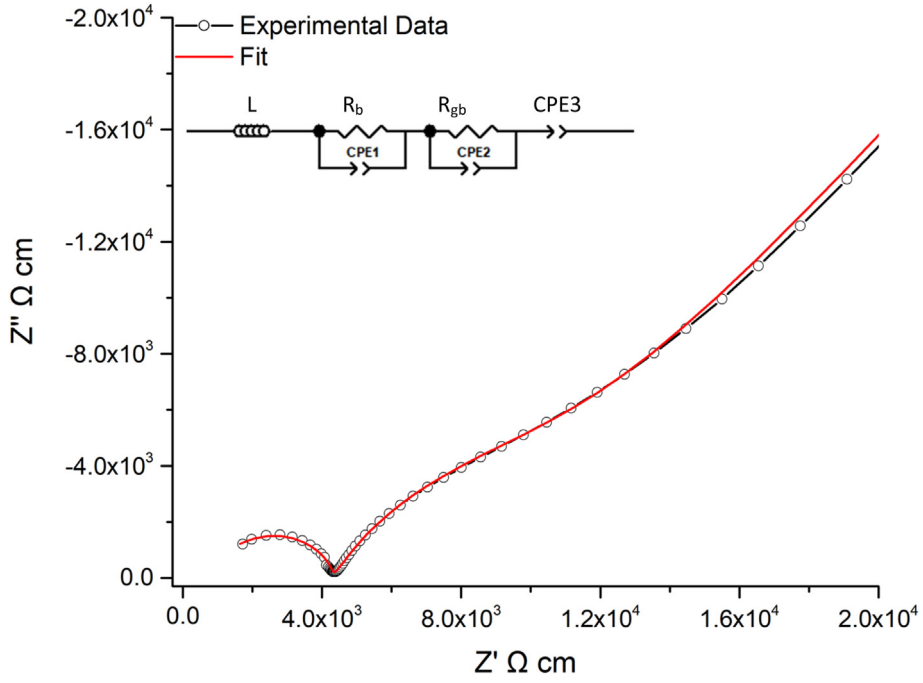

Fig. 5a. HEG1 Nyquist plot at 25 °C demonstrating buried grain boundary contribution. This was fit to the equivalent circuit in the top left.

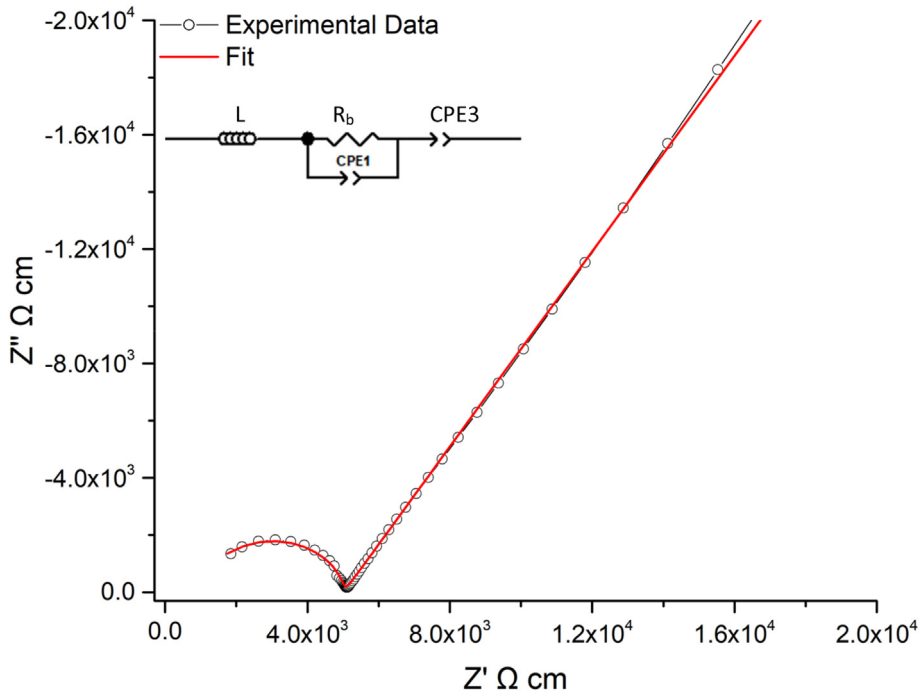

Fig. 5b. HEG2 Nyquist plot at 26 °C demonstrating buried grain boundary contribution. This was fit to the equivalent circuit in the top left and demonstrated overlapping bulk and grain boundary responses.

two parallel R/CPE components (connected in series) to accurately model the system. The denser HEG2 system, by comparison, did not demonstrate any additional contributions, instead fitting to a single R/CPE component in parallel, which corresponds to overlapping bulk/grain boundary contributions, see Fig. 5b. The tail corresponds to the Li transfer resistance at the sample/electrode interface. This arises from the Au which blocks Li diffusion and corresponds to capacitive behaviour due to the formation of space-charge layers. The inductive element is present due to limitations of the setup and has been noted elsewhere in the high frequency range with SSEs [27].

The presence of an additional buried contribution is clearer when the phase angle plots are considered, see Fig. 6a and b. In the high frequency range of both HEG1 and HEG2 a phase angle ~85° is present, which resembles the capacitive behaviour expected within this region (where ideal is 90°). However, a considerably different response is observed in the medium frequency range for HEG1, which has a phase angle of ~65°. This indicates a significant deviance from the expected capacitive behaviour and further indicates a partially buried contribution within the Nyquist plot. These observations are supported further by the spectroscopic C plot. For both phases high frequency plateaus are present with

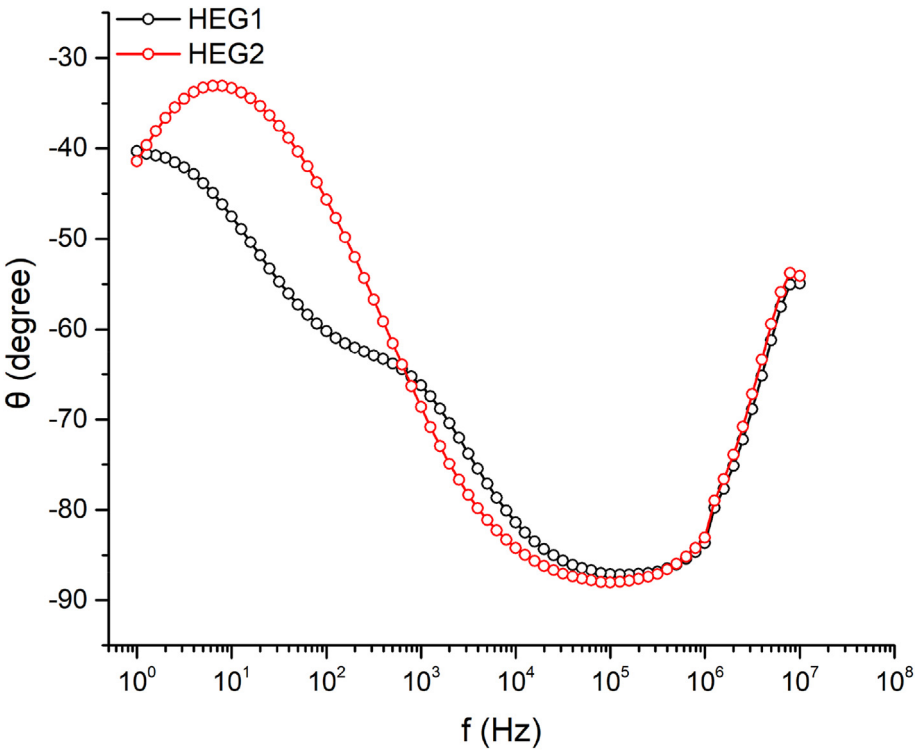

Fig. 6a. Bode plot showing the dependence of phase angle of the two systems, with HEG1 showing considerably difference in the mid-frequency region corresponding to the additional grain boundary response.

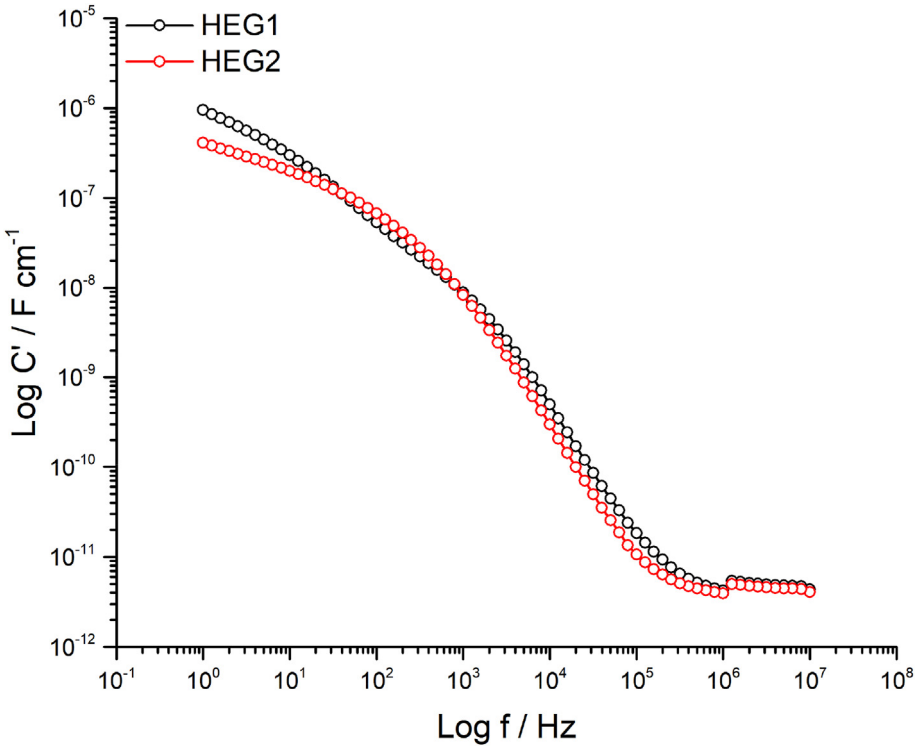

Fig. 6b. Spectroscopic C plot showing high frequency plateaus which in the pF cm^{-1} range which correspond to a bulk oxide response. HEG1 shows additional features ~1000Hz relating the grain boundary component.

capacitance values in the pF cm^{-1} range. This gives dielectric constants between 50 and 60 (based upon the permittivity of free space of 8.854 × 10^{-14} F cm^{-1}). Hence the capacitance values and dielectric constants correspond to the range expected for bulk oxide responses, see Fig. 6 and Table 1 [27,58,66]. HEG1, however, has an additional contribution in the mid frequency region giving capacitance values in ~10^{-8} F cm^{-1} range, indicating a grain boundary response. Therefore, the well resolved semi-circle for HEG1 in Fig. 5a likely corresponds to the bulk response

(0.2 mS cm^{-1}), with the buried contribution being the grain boundary. Therefore, total system conductivity of HEG1 is ~0.1 mS cm^{-1}, see Table 1 and SI for fitted values. The presence of the grain boundary contribution on Fig. 5a is attributed to the decreased density of HEG1 (88%) compared to HEG2 (94%).

The conductivity of both phases falls with ~10^{-4} s cm^{-1}, with HEG2 being slightly better at 0.2 mS cm^{-1}. These are impressive values considering there is only $Li_{5.75}$ *pfu*. Such results are greater than many other, similar, systems and is on par with lithium garnets with larger unit cells and more Li content thus further supporting the favourable properties of increased entropy [27,67–71].

HEG2 was noticeably denser than HEG1, and thus more conductive, hence was analysed further via variable temperature measurements (26–117 °C) to assess activation energy, see Fig. 7. In this case the pellet was painted with Au paste and Au wires attached, as per the methods section. The expected linear dependence was observed and corresponded to a calculated activation energy of 0.33 eV. This is similar to other garnets, therefore indicating the high entropy approach does not alter activation energies. This suggests the hopping pathway is independent of entropic contributions arising from extrinsic defects. Total system conductivity at 103 °C was 3 mS cm^{-1}.

3.4. Symmetrical cell testing

HEG2, being the higher performing system, was subsequently analysed in symmetrical cell form, firstly to analyse the interfacial resistance then to assess galvanostatic lithium plating and stripping stability. Post cell assembly they were analysed via impedance spectroscopy at 20 and 30 °C. The associated Nyquist plot is shown in Fig. 8. The area specific resistance (ASR) for HEG2 was 244 Ω cm^2 at 20 °C (144 Ω cm^2 at 30 °C). These values are lower than our prior reports for Ce-doped LLZO, which suggested partial interfacial Ce reduction led to ASRs of 380 Ω cm^2, but higher than $Ga_{0.2}Li_{6.4}Nd_3Zr_2O_{12}$ (67 Ω cm^2 at room temperature). This may indicate the reduction of ASR with Ce is being enhanced via the Ga and Nd dopants.

The HEG2 symmetric cell was, subsequently, subjected to lithium stripping and plating at 30 °C to assess cycling stability at different current densities, see Fig. 9. HEG2 showed excellent cycling stability with mostly stable voltage profiles over an extended period up to at least 150 μA cm^{-2}. Although some variations in voltage at 150 μA cm^{-2} are present, no large drop in voltage is observed indicative of a short circuit. This shows the HE approach does not compromise the cycling stability of the lithium garnet materials. Furthermore, we reported previously that $Ga_{0.2}Li_{6.4}Nd_3Zr_2O_{12}$ forms a short circuit at 50 μA cm^{-2} but enables low ASR values (67 Ω cm^2) and a high (94%) density. However the strategic use of Ga (0.2 *pfu*) and a smaller amount of Nd (0.5 *pfu*) in HEG2 has enabled much higher current densities while maintaining the favourably high densification and reduction in ASR values previously reported for $Ga_{0.2}Li_{6.4}Nd_3Zr_2O_{12}$, however does so at the cost of Li content due to Li site substitution with Ga and maintaining of charge neutrality [65].

4. Conclusions

In summary, we have shown that lithium garnet materials are very flexible to multi-site dopant strategies, with such dopants enabling relatively easy synthesis despite the elemental complexities involved. We have shown that Li garnet materials can not only handle multiple site substitution simultaneously, but that these sites can also handle several elements at the same time. Although this system is time consuming to weigh out stoichiometrically, the decreased dependency upon a single element could also be economically beneficial. It was also shown that the increased complexity of the garnet system aids in forming of the pure phase, with HEG1 and HEG2 consistently requiring no additional heating steps. It would be of interest to lessen the number of dopants to see if a lower limit can be reached which still enabled such consistency. It would also be of interest to employ more Ln site dopants, such as Ba or Sr to see what properties could be gained from complex Ln site substitution (in addition to increased Li content). An argument arises that Ta and Nb content could be much reduced (therefore increasing Li content) and replaced with increased Ti, as reports suggest dendritic suppression with this dopant [50] whereas use of Fe (on the Li site) has also been shown to alter the garnet symmetry to I4 $\bar{3}$ d. The use of multiple high entropy approaches to produce graded/layered garnet phases, which enable

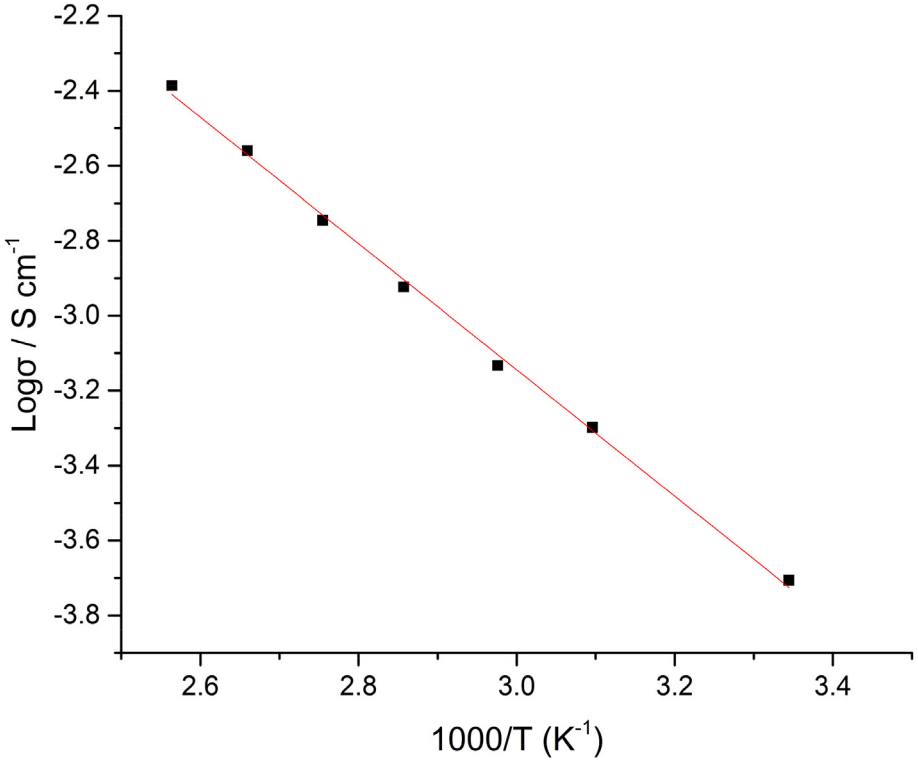

Fig. 7. Arrhenius plot for HEG2 from 26 to 117 °C. Plots show a linear dependence and correspond to an activation energy of 0.33 eV.

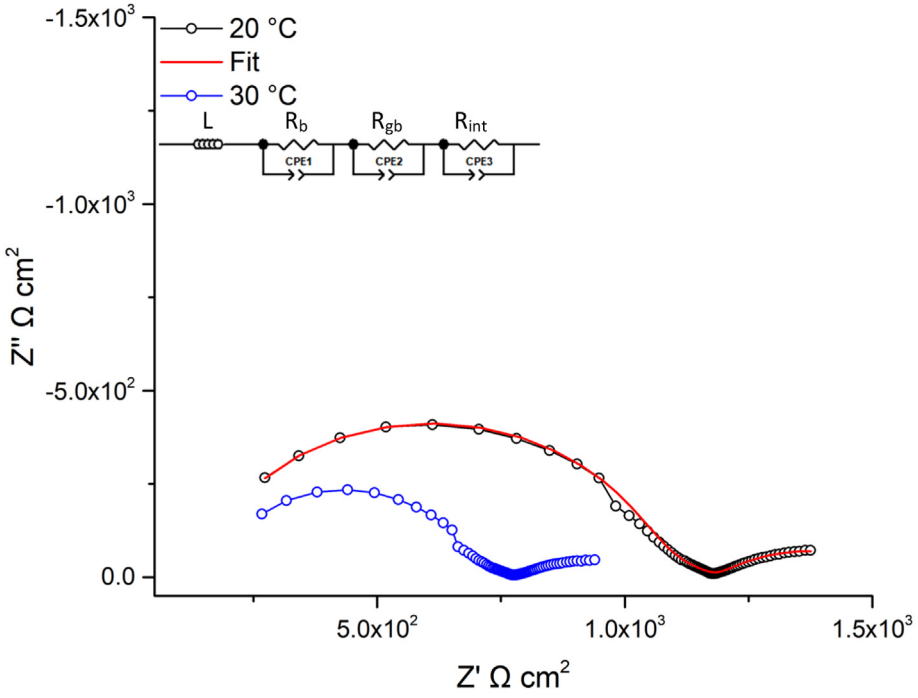

Fig. 8. Li/HEG2/Li symmetrical cell impedance plots at 20 and 30 °C, where the ASR is 224 and 144 Ω cm^2 respectively. Plots are scaled representative the area between the garnet and Li metal, therefore are in ohm cm^2, however conductivity values are similar to what is seen in Fig. 5b.

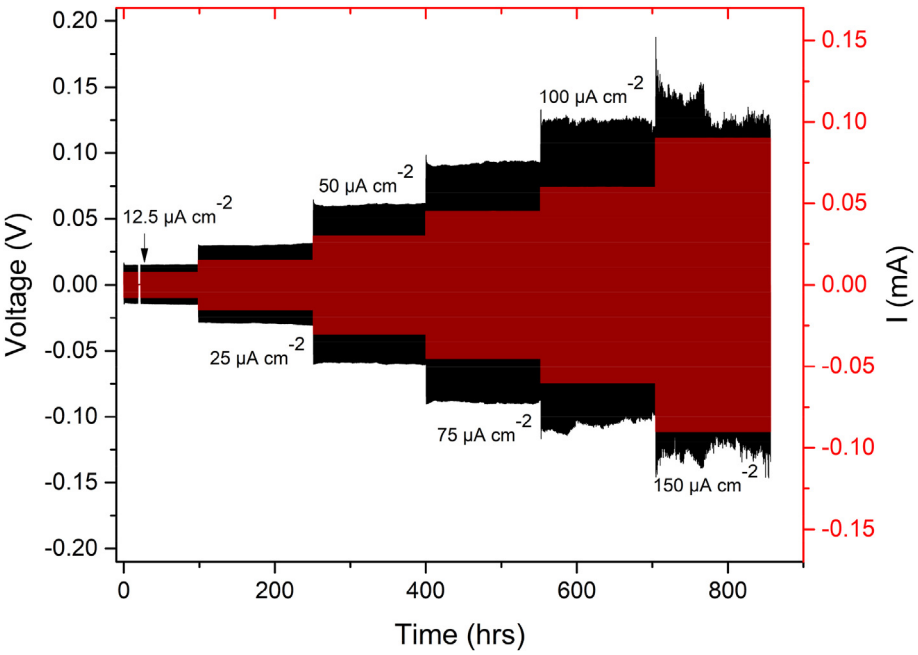

Fig. 9. Li/HEG2/Li symmetrical cell under galvanostatic cycling at 30 °C, indicating mostly flat voltage profiles and excellent cycling stability at several current densities.

different properties at the electrode interface (such as a low ASR) could be a possibility, as would an investigation to see if the high entropy approach is beneficial to use in thin films.

Much work is needed to understand this class of lithium garnets. This cannot be done easily, as the multi-element approach will make distinguishing of structural information a non-trivial task. However, the primary purpose of this work was to demonstrate the possibility of high entropy garnet systems and to push the understanding of the compositional flexibility of these materials. We have additionally shown that these systems show very good conductivity when compared with other garnets with increased Li content and larger lattice parameters. It was also shown that HEGs can exploit a variety of individual dopant properties simultaneously, opening new pathways toward solid state electrolyte engineering.

It is hoped that the exploitation of entropy will enable both better performing materials and provide the basis for more adventurous element combinations. This will allow exploitation of numerous dopants simultaneously, whereupon many are reported to enhance a singular

property (e.g. conductivity, density, interfacial resistance) yet are seldomly used in conjunction. Although the limits of the garnet system have been tested, they have by no means been found. Therefore, there is little reason why further substitution with elements such as Pr, Zn, Ge, Sn, W, Y, Sr and so forth cannot also be considered, with such a strategy possibly being exploited to engineer these materials to achieve optimal performance.

CRediT authorship contribution statement

Mark P. Stockham: Conceptualization, Writing – original draft, Formal analysis, Investigation. **Bo Dong:** Data curation, Investigation. **Peter R. Slater:** Conceptualization, Supervision, Writing – review & editing.

Declaration of competing interest

The authors declare that they have no known competing financial interests or personal relationships that could have appeared to influence the work reported in this paper.

Acknowledgements

We would like to thank the University of Birmingham for the studentship funding of Mark Stockham.

Appendix A. Supplementary data

Supplementary data to this article can be found online at https://doi.org/10.1016/j.jssc.2022.122944.

References

[1] J.M. Tarascon, M. Armand, Issues and challenges facing rechargeable lithium batteries, Nature 414 (2001) 359.
[2] M. Armand, J.M. Tarascon, Building better batteries, Nature 451 (2008) 652.
[3] H. Duan, H. Zheng, Y. Zhou, B. Xu, H. Liu, Stability of garnet-type Li ion conductors: an overview, Solid State Ionics 318 (2018) 45–53.
[4] J.G. Kim, B. Son, S. Mukherjee, N. Schuppert, A. Bates, O. Kwon, M.J. Choi, H.Y. Chung, S. Park, A review of lithium and non-lithium based solid state batteries, J. Power Sources 282 (2015) 299–322.
[5] C. Li, Z.-y. Wang, Z.-j. He, Y.-j. Li, J. Mao, K.-h. Dai, C. Yan, J.-c. Zheng, An advance review of solid-state battery: challenges, progress and prospects, Sustain. Mater. Technol. 29 (2021), e00297.
[6] Q. Liu, Z. Geng, C. Han, Y. Fu, S. Li, Y.-b. He, F. Kang, B. Li, Challenges and perspectives of garnet solid electrolytes for all solid-state lithium batteries, J. Power Sources 389 (2018) 120–134.
[7] Q. Zhao, S. Stalin, C.-Z. Zhao, L.A. Archer, Designing solid-state electrolytes for safe, energy-dense batteries, Nat. Rev. Mater. 5 (3) (2020) 229–252.
[8] C.-X. Zu, H. Li, Thermodynamic analysis on energy densities of batteries, Energy Environ. Sci. 4 (8) (2011) 2614–2624.
[9] N. Nitta, F. Wu, J.T. Lee, G. Yushin, Li-ion battery materials: present and future, Mater. Today 18 (5) (2015) 252–264.
[10] M. Winter, R.J. Brodd, What are batteries, fuel cells, and supercapacitors? Chem. Rev. 104 (10) (2004) 4245–4270.
[11] H. Yang, C. Guo, A. Naveed, J. Lei, J. Yang, Y. Nuli, J. Wang, Recent progress and perspective on lithium metal anode protection, Energy Storage Mater. 14 (2018) 199–221.
[12] Y. Wang, W.D. Richards, S.P. Ong, L.J. Miara, J.C. Kim, Y. Mo, G. Ceder, Design principles for solid-state lithium superionic conductors, Nat. Mater. 14 (2015) 1026.
[13] F. Zheng, M. Kotobuki, S. Song, M.O. Lai, L. Lu, Review on solid electrolytes for all-solid-state lithium-ion batteries, J. Power Sources 389 (2018) 198–213.
[14] C. Bernuy-Lopez, W. Manalastas, J.M. Lopez del Amo, A. Aguadero, F. Aguesse, J.A. Kilner, Atmosphere controlled processing of Ga-substituted garnets for high Li-ion conductivity ceramics, Chem. Mater. 26 (12) (2014) 3610–3617.
[15] F. Flatscher, M. Philipp, S. Ganschow, H.M.R. Wilkening, D. Rettenwander, The natural critical current density limit for Li7La3Zr2O12 garnets, J. Mater. Chem. 8 (31) (2020) 15782–15788.
[16] Y. Zhang, F. Chen, R. Tu, Q. Shen, L. Zhang, Field assisted sintering of dense Al-substituted cubic phase Li7La3Zr2O12 solid electrolytes, J. Power Sources 268 (2014) 960–964.
[17] M. Botros, R. Djenadic, O. Clemens, M. Möller, H. Hahn, Field assisted sintering of fine-grained Li7−3xLa3Zr2AlxO12 solid electrolyte and the influence of the microstructure on the electrochemical performance, J. Power Sources 309 (2016) 108–115.
[18] Federico M. Pesci, R.H. Brugge, A.K.O. Hekselman, A. Cavallaro, R.J. Chater, A. Aguadero, Elucidating the role of dopants in the critical current density for dendrite formation in garnet electrolytes, J. Mater. Chem. 6 (40) (2018) 19817–19827.
[19] F.M. Pesci, A. Bertei, R.H. Brugge, S.P. Emge, A.K.O. Hekselman, L.E. Marbella, C.P. Grey, A. Aguadero, Establishing ultralow activation energies for lithium transport in garnet electrolytes, ACS Appl. Mater. Interfaces 12 (29) (2020) 32806–32816.
[20] R.H. Brugge, F.M. Pesci, A. Cavallaro, C. Sole, M.A. Isaacs, G. Kerherve, R.S. Weatherup, A. Aguadero, The origin of chemical inhomogeneity in garnet electrolytes and its impact on the electrochemical performance, J. Mater. Chem. 8 (28) (2020) 14265–14276.
[21] J. Percival, E. Kendrick, R.I. Smith, P.R. Slater, Cation ordering in Li containing garnets: synthesis and structural characterisation of the tetragonal system, Li7La3Sn2O12, Dalton Trans. (26) (2009) 5177–5181.
[22] E.J. Cussen, T.W.S. Yip, A neutron diffraction study of the d0 and d10 lithium garnets Li3Nd3W2O12 and Li5La3Sb2O12, J. Solid State Chem. 180 (6) (2007) 1832–1839.
[23] E.J. Cussen, The structure of lithium garnets: cation disorder and clustering in a new family of fast Li+ conductors, Chem. Commun. (4) (2006) 412–413.
[24] R. Wagner, G.J. Redhammer, D. Rettenwander, A. Senyshyn, W. Schmidt, M. Wilkening, G. Amthauer, Crystal structure of garnet-related Li-ion conductor Li7−3xGaxLa3Zr2O12: fast Li-ion conduction caused by a different cubic modification? Chem. Mater. 28 (6) (2016) 1861–1871.
[25] J. Awaka, N. Kijima, K. Kataoka, H. Hayakawa, K.-i. Ohshima, J. Akimoto, Neutron powder diffraction study of tetragonal Li7La3Hf2O12 with the garnet-related type structure, J. Solid State Chem. 183 (1) (2010) 180–185.
[26] J. Awaka, N. Kijima, H. Hayakawa, J. Akimoto, Synthesis and structure analysis of tetragonal Li7La3Zr2O12 with the garnet-related type structure, J. Solid State Chem. 182 (8) (2009) 2046–2052.
[27] R.H. Brugge, J.A. Kilner, A. Aguadero, Germanium as a donor dopant in garnet electrolytes, Solid State Ionics 337 (2019) 154–160.
[28] Y.V. Baklanova, A.P. Tyutyunnik, N.V. Tarakina, A.D. Fortes, L.G. Maksimova, D.V. Korona, T.A. Denisova, Stabilization of cubic Li7La3Hf2O12 by Al-doping, J. Power Sources 391 (2018) 26–33.
[29] J. Wolfenstine, J. Ratchford, E. Rangasamy, J. Sakamoto, J.L. Allen, Synthesis and high Li-ion conductivity of Ga-stabilized cubic Li7La3Zr2O12, Mater. Chem. Phys. 134 (2) (2012) 571–575.
[30] B. Dong, M.P. Stockham, P.A. Chater, P.R. Slater, X-ray pair distribution function analysis and electrical and electrochemical properties of cerium doped Li5La3Nb2O12 garnet solid-state electrolyte, Dalton Trans. 49 (33) (2020) 11727–11735.
[31] M.P. Stockham, B. Dong, Y. Ding, Y. Li, P.R. Slater, Evaluation of the effect of site substitution of Pr doping in the lithium garnet system Li5La3Nb2O12, Dalton Trans. (2020).
[32] M.P. Stockham, B. Dong, M.S. James, Y. Li, Y. Ding, P.R. Slater, Water based synthesis of highly conductive GaxLi7−3xLa3Hf2O12 garnets with comparable critical current density to analogous GaxLi7−3xLa3Zr2O12 systems, Dalton Trans. 50 (7) (2021) 2364–2374.
[33] B. Dong, L.L. Driscoll, M.P. Stockham, E. Kendrick, P.R. Slater, Low temperature synthesis of garnet solid state electrolytes: implications on aluminium incorporation in Li7La3Zr2O12, Solid State Ionics 350 (2020) 115317.
[34] J.L. Allen, J. Wolfenstine, E. Rangasamy, J. Sakamoto, Effect of substitution (Ta, Al, Ga) on the conductivity of Li7La3Zr2O12, J. Power Sources 206 (2012) 315–319.
[35] S.W. Xin, M. Zhang, T.T. Yang, Y.Y. Zhao, B.R. Sun, T.D. Shen, Ultrahard bulk nanocrystalline VNbMoTaW high-entropy alloy, J. Alloys Compd. 769 (2018) 597–604.
[36] B. Wu, Z. Xie, J. Huang, J. Lin, Y. Yang, L. Jiang, J. Huang, G. Ye, C. Zhao, S. Yang, B. Sa, Microstructures and thermodynamic properties of high-entropy alloys CoCrCuFeNi, Intermetallics 93 (2018) 40–46.
[37] Naeem, M.; He, H.; Zhang, F.; Huang, H.; Harjo, S.; Kawasaki, T.; Wang, B.; Lan, S.; Wu, Z.; Wang, F.; Wu, Y.; Lu, Z.; Zhang, Z.; Liu Chain, T.; Wang, X.-L., Cooperative deformation in high-entropy alloys at ultralow temperatures. Sci. Adv. 6 (13), eaax4002.
[38] J.W. Yeh, S.K. Chen, S.J. Lin, J.Y. Gan, T.S. Chin, T.T. Shun, C.H. Tsau, S.Y. Chang, Nanostructured high-entropy alloys with multiple principal elements: novel alloy design concepts and outcomes, Adv. Eng. Mater. 6 (5) (2004) 299–303.
[39] E.P. George, D. Raabe, R.O. Ritchie, High-entropy alloys, Nat. Rev. Mater. 4 (8) (2019) 515–534.
[40] J.-W. Yeh, Alloy design strategies and future trends in high-entropy alloys, JOM 65 (12) (2013) 1759–1771.
[41] M.-H. Tsai, J.-W. Yeh, High-entropy alloys: a critical review, Mater. Res. Lett. 2 (3) (2014) 107–123.
[42] Y. Zhang, T.T. Zuo, Z. Tang, M.C. Gao, K.A. Dahmen, P.K. Liaw, Z.P. Lu, Microstructures and properties of high-entropy alloys, Prog. Mater. Sci. 61 (2014) 1–93.
[43] D.J.M. King, S.C. Middleburgh, A.G. McGregor, M.B. Cortie, Predicting the formation and stability of single phase high-entropy alloys, Acta Mater. 104 (2016) 172–179.
[44] M.C. Troparevsky, J.R. Morris, M. Daene, Y. Wang, A.R. Lupini, G.M. Stocks, Beyond atomic sizes and Hume-Rothery rules: understanding and predicting high-entropy alloys, JOM 67 (10) (2015) 2350–2363.
[45] Z. Lun, B. Ouyang, D.-H. Kwon, Y. Ha, E.E. Foley, T.-Y. Huang, Z. Cai, H. Kim, M. Balasubramanian, Y. Sun, J. Huang, Y. Tian, H. Kim, B.D. McCloskey, W. Yang, R.J. Clément, H. Ji, G. Ceder, Cation-disordered rocksalt-type high-entropy cathodes for Li-ion batteries, Nat. Mater. 20 (2) (2021) 214–221.

[46] C. Zhao, F. Ding, Y. Lu, L. Chen, Y.-S. Hu, High-entropy layered oxide cathodes for sodium-ion batteries, Angew. Chem. Int. Ed. 59 (1) (2020) 264–269.
[47] Q. Wang, A. Sarkar, D. Wang, L. Velasco, R. Azmi, S.S. Bhattacharya, T. Bergfeldt, A. Düvel, P. Heitjans, T. Brezesinski, H. Hahn, B. Breitung, Multi-anionic and -cationic compounds: new high entropy materials for advanced Li-ion batteries, Energy Environ. Sci. 12 (8) (2019) 2433–2442.
[48] Shijie, Z.; Na, L.; Liping, S.; Qiang, L.; Lihua, H.; Hui, Z., A novel high-entropy cathode with the A2BO4-type structure for solid oxide fuel cells. J. Alloys Compd. 2021, 162548.
[49] V. Thangadurai, H. Kaack, W.J.F. Weppner, Novel fast lithium ion conduction in garnet-type Li5La3M2O12 (M = Nb, Ta), J. Am. Ceram. Soc. 86 (3) (2004) 437–440.
[50] J. Gao, J. Zhu, X. Li, J. Li, X. Guo, H. Li, W. Zhou, Rational design of mixed electronic-ionic conducting Ti-doping Li7La3Zr2O12 for lithium dendrites suppression, Adv. Funct. Mater. 31 (2) (2021) 2001918.
[51] M.P. Stockham, B. Dong, M.S. James, Y. Li, Y. Ding, E. Kendrick, P.R. Slater, Evaluation of Ga0.2Li6.4Nd3Zr2O12 garnets: exploiting dopant instability to create a mixed conductive interface to reduce interfacial resistance for all solid state batteries, Dalton Trans. 50 (39) (2021) 13786–13800.
[52] B. Dong, S.R. Yeandel, P. Goddard, P.R. Slater, Combined experimental and computational study of Ce-doped La3Zr2Li7O12 garnet solid-state electrolyte, Chem. Mater. 32 (1) (2020) 215–223.
[53] M.C. Troparevsky, J.R. Morris, P.R.C. Kent, A.R. Lupini, G.M. Stocks, Criteria for predicting the formation of single-phase high-entropy alloys, Phys. Rev. X 5 (1) (2015), 011041.
[54] R. Jalem, Y. Morishita, T. Okajima, H. Takeda, Y. Kondo, M. Nakayama, T. Kasuga, Experimental and first-principles DFT study on the electrochemical reactivity of garnet-type solid electrolytes with carbon, J. Mater. Chem. 4 (37) (2016) 14371–14379.
[55] A. Gupta, R. Murugan, M.P. Paranthaman, Z. Bi, C.A. Bridges, M. Nakanishi, A.P. Sokolov, K.S. Han, E.W. Hagaman, H. Xie, C.B. Mullins, J.B. Goodenough, Optimum lithium-ion conductivity in cubic Li7−xLa3Hf2−xTaxO12, J. Power Sources 209 (2012) 184–188.
[56] S. Mukhopadhyay, T. Thompson, J. Sakamoto, A. Huq, J. Wolfenstine, J.L. Allen, N. Bernstein, D.A. Stewart, M.D. Johannes, Structure and stoichiometry in supervalent doped Li7La3Zr2O12, Chem. Mater. 27 (10) (2015) 3658–3665.
[57] B. Toby, R. Dreele, GSAS-II: the genesis of a modern open-source all-purpose crystallography software package, J. Appl. Crystallogr. 46 (2013) 544–549.
[58] R.H. Brugge, A.K.O. Hekselman, A. Cavallaro, F.M. Pesci, R.J. Chater, J.A. Kilner, A. Aguadero, Garnet electrolytes for solid state batteries: visualization of moisture-induced chemical degradation and revealing its impact on the Li-ion dynamics, Chem. Mater. 30 (11) (2018) 3704–3713.
[59] G. Larraz, A. Orera, M.L. Sanjuán, Cubic phases of garnet-type Li7La3Zr2O12: the role of hydration, J. Mater. Chem. 1 (37) (2013) 11419–11428.
[60] C. Galven, J. Dittmer, E. Suard, F. Le Berre, M.-P. Crosnier-Lopez, Instability of lithium garnets against moisture. Structural characterization and dynamics of Li7-xHxLa3Sn2O12 and Li5-xHxLa3Nb2O12, Chem. Mater. 24 (17) (2012) 3335–3345.
[61] J. Percival, D. Apperley, P.R. Slater, Synthesis and structural characterisation of the Li ion conducting garnet-related systems, Li6ALa2Nb2O12 (A=Ca, Sr), Solid State Ionics 179 (27) (2008) 1693–1696.
[62] M.A. Howard, O. Clemens, E. Kendrick, K.S. Knight, D.C. Apperley, P.A. Anderson, P.R. Slater, Effect of Ga incorporation on the structure and Li ion conductivity of La3Zr2Li7O12, Dalton Trans. 41 (39) (2012) 12048–12053.
[63] H. Peng, Y. Zhang, L. Li, L. Feng, Effect of quenching method on Li ion conductivity of Li5La3Bi2O12 solid state electrolyte, Solid State Ionics 304 (2017) 71–74.
[64] N. Hamao, K. Kataoka, J. Akimoto, Li-ion Conductivity and Crystal Structure of Garnet-type Li6.5La3M1.5Ta0.5O12 (M = Hf, Sn) Oxides, 125, 2017, pp. 272–275.
[65] M.P. Stockham, B. Dong, M.S. James, Y. Li, Y. Ding, E. Kendrick, P. Slater, Evaluation of Ga0.2Li6.4Nd3Zr2O12 garnets: exploiting dopant instability to create a mixed conductive interface to reduce interfacial resistance for all solid state batteries, Dalton Trans. (2021).
[66] S. Narayanan, A.K. Baral, V. Thangadurai, Dielectric characteristics of fast Li ion conducting garnet-type Li5+2xLa3Nb2−xYxO12 (x = 0.25, 0.5 and 0.75), Phys. Chem. Chem. Phys. 18 (22) (2016) 15418–15426.
[67] J. Percival, P.R. Slater, Identification of the Li sites in the Li ion conductor, Li6SrLa2Nb2O12, through neutron powder diffraction studies, Solid State Commun. 142 (6) (2007) 355–357.
[68] H. Buschmann, J. Dölle, S. Berendts, A. Kuhn, P. Bottke, M. Wilkening, P. Heitjans, A. Senyshyn, H. Ehrenberg, A. Lotnyk, V. Duppel, L. Kienle, J. Janek, Structure and dynamics of the fast lithium ion conductor "Li7La3Zr2O12", Phys. Chem. Chem. Phys. 13 (43) (2011) 19378–19392.
[69] M.A. Howard, O. Clemens, K.S. Knight, P.A. Anderson, S. Hafiz, P.M. Panchmatia, P.R. Slater, Synthesis, conductivity and structural aspects of Nd3Zr2Li7−3xAlxO12, J. Mater. Chem. 1 (44) (2013) 14013–14022.
[70] Y. Matsuda, A. Sakaida, K. Sugimoto, D. Mori, Y. Takeda, O. Yamamoto, N. Imanishi, Sintering behavior and electrochemical properties of garnet-like lithium conductor Li6.25M0.25La3Zr2O12 (M: Al3+ and Ga3+), Solid State Ionics 311 (2017) 69–74.
[71] R. Murugan, V. Thangadurai, W. Weppner, Fast lithium ion conduction in garnet-type Li7La3Zr2O12, Angew. Chem. Int. Ed. 46 (41) (2007) 7778–7781.